Adaptive Human Force Scaling via Admittance Control for Physical Human-Robot Interaction

Yahya M. Hamad, Yusuf Aydin, *Member, IEEE*, and Cagatay Basdogan, *Member, IEEE*

***Abstract*—The goal of this article is to design an admittance controller for a robot to adaptively change its contribution to a collaborative manipulation task executed with a human partner to improve the task performance. This has been achieved by adaptive scaling of human force based on her/his movement intention while paying attention to the requirements of different task phases. In our approach, movement intentions of human are estimated from measured human force and velocity of manipulated object, and converted to a quantitative value using a fuzzy logic scheme. This value is then utilized as a variable gain in an admittance controller to adaptively adjust the contribution of robot to the task without changing the admittance time constant. We demonstrate the benefits of the proposed approach by a pHRI experiment utilizing Fitts' reaching movement task. The results of the experiment show that there is a) an optimum admittance time constant maximizing the human force amplification and b) a desirable admittance gain profile which leads to a more effective co-manipulation in terms of overall task performance.**

***Index Terms*—Physical human-robot interaction, collaborative manipulation, adaptive force amplification, admittance control, human intention, Fitts' task.**

I. Introduction

HUMAN and robot, working together, are expected to play an important role in the foreseeable future. The increasing demand for high-quality and more flexible systems to carry out complex tasks put this dyad firmly in the field. Integrating human's dexterity and problem-solving skills along with robot's precision, strength, and repeatability into tasks involving physical interaction between them, pHRI, could be quite beneficial. Such a collaborative interaction may result in significant improvements in task performance and reduction in physical human effort [1]–[6].

In order to make pHRI more effective, we need robots to anticipate the human partner's intentions and act accordingly [7]. In this regard, one of the sensory channels that flourish in nowadays is haptics [8]. For example, if we consider a collaborative object manipulation task (see Fig. 1), the direction of force applied by human operator can be used to set the intended direction of object movement, while its magnitude can be used to regulate the movement speed of the object by robot.

To this end, interaction controllers (admittance or its reciprocal, impedance controllers) are commonly utilized to regulate the physical interaction between human and robot. In general, it is more natural to utilize admittance controller when robots used in pHRI do not possess high back drivability and force control. As such robots are usually motion-controlled, the force applied by human can serve as the input to admittance controller, which computes the reference motion trajectory for the manipulated object.

Although admittance controllers have been used in pHRI studies in the past, the use of a standard admittance controller in which controller parameters are fixed has some limitations. A standard admittance controller may not be flexible enough to the changes in human intentions and task requirements, which happen frequently during the execution of a collaborative task. The changes in human intention due to varying requirements of a task typically suggest that human expects either more resistive or more compliant behavior from robot. For instance, collaborative manipulation of an object typically involves three main phases, which demands different behaviors from robot in those phases; human initializes the motion (i.e. starting phase), guides the robot to bring the object closer to a target location (i.e. driving phase), and then precisely positions it to park at that location (i.e. parking phase). Initially, the task requires a rapid reaction from the robot while avoiding a jerky behavior, hence, an admittance controller having moderate dissipation capacity might be more desirable at this stage. Thereafter, during driving the manipulated object, lower dissipation capacity is preferred to promote acceleration, and hence to reduce the overall task duration and human effort. Following, as the object gets closer to the target location, increasing the dissipation gradually is needed to decelerate the object. While parking the object, maximizing the precision is more critical than reducing human effort. Human operator naturally stiffens her/his arm muscles to park the object precisely, which may degrade the stability of pHRI. In this phase of the task, if the controller parameters are adjusted to dissipate more energy, not only the stability but also the parking precision is improved.

Consequently, an adaptive admittance controller where controller parameters are no longer fixed may adapt better to

Manuscript received September 24, 2020; revised February 26, 2021; accepted March 26, 2021. Date of publication April 7, 2021; date of current version December 16, 2021. This article was recommended for publication by Associate Editor Dr. Matteo Bianchi and Editor-in-Chief Prof. Domenico Prattichizzo upon evaluation of the reviewers' comments. *(Corresponding author: Cagatay Basdogan.)*

Yahya M. Hamad is with the College of Engineering, Koc University, Istanbul 34450, Turkey, and also with the Al-Khwarizmi College of Engineering, University of Baghdad, Baghdad 10071, Iraq (e-mail: yalqaysi13@ku.edu.tr).

Yusuf Aydin is with the Faculty of Engineering, MEF University, Istanbul 34396, Turkey (e-mail: aydiny@mef.edu.tr).

Cagatay Basdogan is with the College of Engineering, Koc University, Istanbul 34450, Turkey (e-mail: cbasdogan@ku.edu.tr).

Digital Object Identifier 10.1109/TOH.2021.3071626

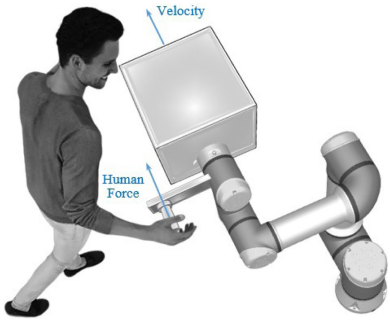

Fig. 1. Human-robot co-manipulation scenario.

varying needs of human operator in pHRI. However, as the physical strength of human is limited in performing some pHRI tasks such as manipulating heavy objects, it is required to further exploit robot's strength. In such a case, human applies some force to the object for guidance, while robot scales up this force to help with its manipulation [9], [10]. On the other hand, in some other applications, such as robot-assisted micro surgery, where only small forces are expected to be applied to the manipulated object, human force attenuation is desired [11].

In this study, we propose an approach for human force scaling to adaptively change the contribution of robot to a collaborative manipulation task in order to improve the task performance. In our approach, movement intentions of human are estimated from measured human force and velocity of manipulated object, and converted to a quantitative index using a fuzzy logic scheme. This index is then utilized as a variable gain in an admittance controller to scale up/down the force applied by robot to the object. In essence, such an approach is similar to the adaptive admittance controller, but here, the gain contribution of the controller, not just the parameters of it, is varied. In order to adjust the contribution of robot, a frequently utilized approach in literature is to alter the dissipation capacity of the admittance controller by varying the admittance damping, but this also affects the time constant of the controller. On the other hand, our approach allows to change the gain contribution of the controller alone without changing its time constant. Therefore, the proposed approach enables a direct control of both the gain and time constant of an admittance controller, which provides flexibility in achieving different goals at different stages of a pHRI task, leading to an improvement in overall task performance.

A. Related Work

There are already studies in the literature on estimation of human intention to regulate an interaction controller for intuitive pHRI. For instance, Ikeura *et al.* [12] utilized the velocity of manipulated object to alter the damping parameter of a variable admittance controller. In their approach, if the magnitude of object velocity was higher (lower) than a threshold value, human was assumed to speed up (slow down), and hence, the admittance damping was set to a low (high) value to promote (damp) the motion. Kang *et al.* [13] used object velocity to estimate human intention as to accelerate (decelerate) the object. Accordingly, when human force exceeded a certain threshold value, admittance damping was decreased (increased) as the object velocity increased (decreased). Tsumugiwa *et al.* [14] and Rahman *et al.* [15] estimated human arm stiffness and adjusted the admittance damping on-the-fly in proportion to the estimated stiffness and depending on some velocity thresholds. In [16]–[18], human intention was estimated based on the measurement of muscle activation of human arm via EMG sensors to provide effective assistance in co-manipulation tasks. Keemink *et al.* [19] proposed a position-dependent admittance damping for co-manipulation of heavy objects and investigated its effect on the accuracy of object positioning, reaching time, and magnitude of force applied by human. Starting from a low value, they increased the damping between starting and target locations as a linear function of position. The methods suggested in [12]–[15], [19] relied on either some velocity or force thresholds, or position of the manipulated object, which are task-dependent information, restricting the practical use of such methods. Also, the estimation of human arm stiffness in [14] and [15] requires additional computational effort, which is not trivial if pHRI task is complex. Similarly, utilizing EMG sensors for intent detection is not very practical [16]–[18], since it requires to attach them to user's arm.

There are several studies in the literature utilizing the force-based information to infer the human intention as well. For instance, Li *et al.* [20], [21] utilized force applied by human to interpret human intention to adjust the controller parameters accordingly. In their approach, damping was increased to improve accuracy (decreased for more compliance), when the human force was low (high). Duchaine and Gosselin [22] and Duchaine *et al.* [23] utilized the derivative of the force applied by human and the velocity of manipulated object together to predict whether human intends to accelerate or decelerate the object. Aydin *et al.* [24] improved the approach proposed in [22] by adding a fuzzy-based intention estimator. Instead of using the derivative of interaction force, Lecours *et al.* [25] preferred the acceleration output of admittance controller directly, so that the noise in force measurement would not adversely affect the intention estimation. They used the admittance acceleration in tandem with the velocity of manipulated object to estimate whether human intends to accelerate or decelerate the object. Dimeas and Aspragathos [26] proposed a fuzzy-based online adaptation technique that utilizes the end-effector velocity of robot and force applied by human to alter the admittance damping. In [22]–[26], admittance damping was increased or decreased when the human intention was estimated as deceleration or acceleration, respectively.

In some pHRI applications, researchers have relied on amplification (attenuation) of human force to increase (decrease) the contribution of robot to the collaborative task [11], [27]–[29]. A well-known example in this group is exoskeletons [9], [30]–[32] which are designed to amplify human force. This approach has applications in different domains including rehabilitation, military, and industry. In the studies listed above, amplification (attenuation) is achieved by first scaling up (down) the forces applied by human and then feeding it to an admittance controller to generate a velocity command for the robot interacting with the environment.

However, force scaling approaches used in those studies typically utilize constant amplification/attenuation gain. We believe that an adaptive force scaling, based on human intention, may result in improvements in task performance for pHRI tasks that involve even no contact interactions with an environment such as collaborative manipulation of objects.

B. Contributions

In earlier pHRI studies [12]–[26], adaptive approaches based on human intention have been investigated to alter parameters of an interaction controller. In those studies, human intent has been typically interpreted as "acceleration" or "deceleration" without paying sufficient attention to different phases of a pHRI task (i.e. sub-tasks). However, as explained earlier, each phase of a pHRI task requires different actions from the controller, so the desired behavior under the specific phase can be achieved. Therefore, we argue that adaptive scaling of human force based on not only the human intention but also the task phases, such as starting, driving, and parking in object manipulation, would further enhance the quality of pHRI.

Although there are several studies in the pHRI literature aiming to reduce human effort and task performance, to our knowledge, adaptive scaling of human force using an admittance controller has not been proposed for collaborative manipulation of a heavy/bulky object. In our approach, human intention as to accelerate or decelerate a manipulated object is estimated by a rule-based approach and converted to a quantitative index using a fuzzy logic scheme. This index is then integrated over time to accommodate the different requirements of each manipulation phase. Finally, the integrated value at each time step is used to alter the gain of an admittance controller on the fly for adaptive scaling of human force.

Using the proposed approach, we investigate a) if there is an optimal admittance time constant that maximizes human force amplification and b) if the resulting admittance gain profile leads to a further enhancement in a co-manipulation performance than the ones suggested in the literature.

The rest of this article is organized as follows: Section II introduces the admittance controller architecture utilized in this study. Section III presents the proposed adaptation approach including the estimation of human intention index and how this index is used to modulate the gain of an admittance controller to adjust the contribution of robot to the task. The stability limits for the coupled system, the permissible range for the force amplification, and the selection of optimal time constant for the admittance controller are all discussed in Section IV. Section V presents the details of a pHRI experiment involving Fitts' reaching movement task, which was conducted to investigate the potential benefits of the proposed approach. Section VI summarizes the experimental results and provides a discussion of the study. Conclusions and future research directions are given in Section VII.

II. Control Architecture

In our approach, we assume that human and robot are coupled as shown in Fig. 1 and manipulate an object together. The admittance control architecture suggested for this purpose is depicted in Fig. 2. Here, human exerts a force to move the object with a desired velocity $v_{\rm des}$. The force applied by human f_H is measured by a force sensor, amplified by a gain G_H and then sent to the admittance controller $Y(s)$ of robot to adjust its contribution to the task. The admittance controller outputs a reference velocity $v_{\rm ref}$ for the motion controller of robot.

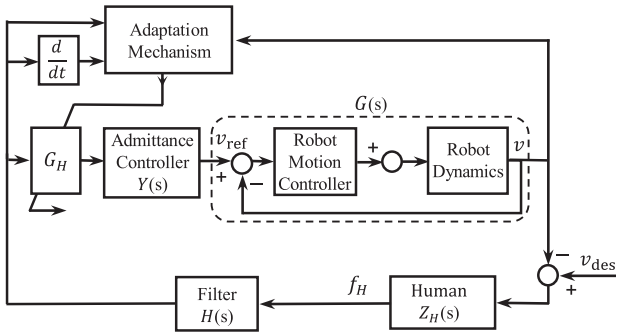

Fig. 2. Control architecture for the pHRI system.

The inner motion controller of robot transmits sufficient torques to its joints to move the object with a velocity of v. We assume that robot motion controller is robust enough such that the actual velocity of the robot v is not significantly affected by environmental forces [33], [34]. Then, the transfer function $T(s)$ of the main pHRI closed-loop system in Fig. 2 is given by:

$$T(s) = \frac{V(s)}{F_H(s)} = \frac{G_H Y(s) G(s) H(s)}{1 + G_H Y(s) G(s) H(s) Z_H(s)} \quad (1)$$

where $V(s)$ and $F_H(s)$ are the Laplace transformations of v and f_H, respectively. Here, $H\ (s) = \ (0.1122\ s + 31.75)/(s + 31.75)$ represents the model of a low pass filter applied to the measured human force, $Z_H(s)$ represents the impedance of human arm, and $G\ (s) = V(s)/V_{ref}(s)$ is the transfer function for robot [34], where $V_{ref}(s)$ is the Laplace transformation of v_{ref}. Note that all the variables introduced here are scalars as the study focuses on a one-dimensional co-manipulation task (see Section V).

Admittance controller: In typical implementation of an admittance controller for a pHRI task involving a collaborative object manipulation, a linear model of the following form is utilized (note that a spring element is not preferred as it forces the robot to return to an equilibrium position, which is not desirable):

$$Y(s) = \frac{V_{\rm ref}(s)}{F_H(s)} = \frac{1}{m_a s + b_a} \quad (2)$$

where m_a and b_a represent the admittance mass and damping, respectively. Eq. (2) can be rearranged as,

$$Y(s) = \frac{K_a}{\tau_a s + 1} \quad (3)$$

where, $K_a\ = 1/b_a$ is the admittance gain and $\tau_a = \ m_a/b_a$ is the admittance time constant. In this study, we alter the admittance gain to adjust the contribution of the robot to the task while keeping the time constant of the controller unchanged. Note that increasing (decreasing) the admittance gain decreases (increases) the energy dissipation of the controller.

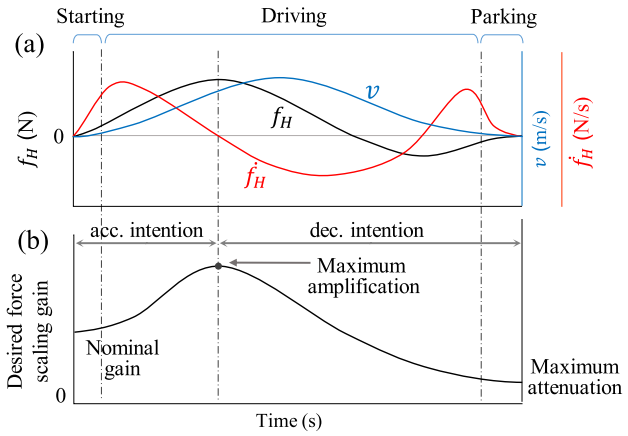

Fig. 3. (a) Representative profiles of object velocity v, force applied by human f_H, and its derivative $\dot{f}_H$, and (b) desired force scaling gain profile for a co-manipulation task.

Tuning of admittance parameters with constant ratio of m_a/b_a has been proposed in [25], but we investigate its optimum value in this study.

III. Approach

Recalling the co-manipulation scenario discussed earlier, different control actions should be considered for each phase of the task. To further illustrate these phases, we consider a one-dimensional co-manipulation task. We assume that human operator and a robot collaboratively transport an object having high inertia along a straight path from a starting position to a target position which is unknown to the robot a priori. Utilizing the control architecture given in previous section, robot manipulates the object under the guidance of forces applied by the human operator. For such a task, representative profiles for the velocity of manipulated object, force applied by human, and its derivative are depicted as functions of time in Fig. 3a. As anticipated, there is a phase delay between force and velocity when the inertia of the object is relatively high. For the same reason, when such an object is already in motion, reversing the force direction to decelerate it requires additional human effort.

Considering Fig. 3a, if velocity is close to zero, velocity and force vectors are both in the same direction, and also force rate (i.e., derivative of force) is increasing in the same direction, we can argue that human intends to initialize the movement to accelerate the object (i.e., starting phase). When the velocity is sufficiently high, we can say that driving phase is being executed. If the velocity is close to zero again but force and force rate are in opposite directions, we can assume that human intends to park the object to the target location. Based on the description above, one can carefully design a profile for the admittance gain to satisfy the requirements of each phase. Such a profile is given in Fig. 3b. The gain starts from a nominal value and increases slowly during the starting phase. In the driving phase, the dissipative (i.e., resistive) behavior of robot should be avoided as human desires to accelerate the object easily. At some point during this phase, human intends to decelerate the object (note that if the object has large inertia, it may continue to accelerate as in Fig. 3a; force magnitude starts to decay indicating human desires to decelerate the object though the velocity continues to increase). From this point on (see the maximum amplification point in Fig. 3b), the dissipation capacity of the controller should be increased based on how much human intends to decelerate.

In order to achieve a gain profile similar to the one proposed in Fig. 3b, we first estimate human movement intention as to accelerate or decelerate using a rule-based approach and then quantify it by a numerical value using a fuzzy logic scheme. We then integrate this value along the movement trajectory while bounding it by a logistic sigmoid function to comply with the different requirements of each task phase.

A. Estimation of Human Intention

In earlier studies, either velocity of the manipulated object and the derivative of force applied by the human [22]–[24] or velocity and force [26] were used to estimate human intention as to either accelerate or decelerate the object. In our approach, we utilize all three of them to estimate human intention and quantify it by a numerical value called as Human Intention Index (K_{HII}). All three are needed to carefully detect the human intention during the driving phase, especially when manipulating a heavy object at a high speed. Towards the end of this phase, human reverses the force direction to dissipate the generated kinetic energy in order to park the object successfully without an overshoot in the next phase. If we use force derivative and velocity only, then human intention would be detected incorrectly as acceleration during the parking phase (Fig. 3a). On the other hand, if we use force and velocity only, then the detection of deceleration intention will be delayed.

Fig. 4a shows our approach for estimating human intention. First, the features are fed to a fuzzy logic scheme which generates K_{HII}. This scheme outputs a value representing human intention as to accelerate $(0 < K_{\mathrm{HII}} \leq 1)$ or decelerate $(-1 \leq K_{\mathrm{HII}} < 0)$ the manipulated object. Each input and the output consist of three normalized triangular membership functions (positive, intermediate, and negative). The Mamdani fuzzy inference system is utilized, and the intention rules described in (4) are implemented. A representative profile of K_{HII} as a function of time is depicted in Fig. 4b.

$$\begin{array}{lcl} v.\dot{f}_H > 0 & \Rightarrow & \left\{ \begin{array}{l} v.f_H > 0 \Rightarrow \ Intent: \ acc. \\ v.f_H < 0 \Rightarrow \ Intent: \ dec. \end{array} \right\} \\ v.\dot{f}_H < 0 & \Rightarrow & \{Intent: \ dec.\} \\ v.\dot{f}_H \approx 0 & \Rightarrow & \{Intent: \ no \ change\} \end{array} \tag{4}$$

A further processing on K_{HII} is needed to obtain the desired gain profile depicted in Fig. 3b. To this end, a simple discrete integration of K_{HII} is a practical solution. Note that derivative of force, which is typically noisy, is utilized in the computation of K_{HII}, hence such integration accumulates the index values on-the-fly, producing a profile that is not only similar to the desired gain profile but also robust to noise.

Hence, the integrated human intention index is obtained using the following equation:

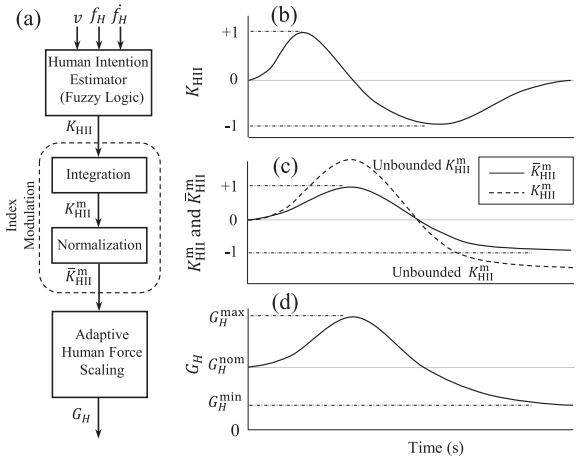

Fig. 4. (a) Proposed adaptation mechanism, and the representative profiles for (b) human intention index K_{HII}, (c) integrated ($K^{\mathrm{m}}_{\mathrm{HII}}$) and bounded ($\bar{K}^{\mathrm{m}}_{\mathrm{HII}}$) human intention indices, and (d) desired gain (G_H).

$$K^{\mathrm{m}}_{\mathrm{HII}}\ (t) = K^{\mathrm{m}}_{\mathrm{HII}}\ (t-1) +\ K_{\mathrm{HII}}(t)\ \alpha\ \Delta t \tag{5}$$

where, α is the integration constant used to control the rate of accumulation and to reduce the delay in gain adaptation, and Δt is the sampling time.

Due to the integration process, $K^{\mathrm{m}}_{\mathrm{HII}}$ might reach to large values. A logistic sigmoid function is utilized in this study to obtain a bounded value as (see Fig. 4c):

$$\bar{K}^{\mathrm{m}}_{\mathrm{HII}}(\mathrm{t})\ =\ -1+2\left(\frac{1}{1+\mathrm{e}^{-K^{\mathrm{m}}_{\mathrm{HII}}(\mathrm{t})}}\right) \tag{6}$$

B. Adaptive Human Force Scaling

In our design, when the operator intends to accelerate the object, the force scaling gain G_H, which is applied to the measured human force to adapt the contribution of robot to the co-manipulation task, increases from its nominal value G^{nom}_H until reaching to its maximum allowable limit G^{max}_H (i.e., $G^{\mathrm{nom}}_H \leq G_H \leq G^{\mathrm{max}}_H$). Hence, more assistance is provided to human during acceleration. When deceleration intention is detected, G_H decreases from its current value toward the minimum limit G^{min}_H, which is below the nominal value (i.e., $G^{\mathrm{min}}_H \leq G_H < G^{\mathrm{nom}}_H$). In order to make the transition smoother, the scaling gain is calculated as (see Fig. 4d):

$$G_H(t) = G^{\mathrm{nom}}_H\ +\ I_H\ \bar{K}^{\mathrm{m}}_{\mathrm{HII}}(\mathrm{t}) \tag{7}$$

Here, $I_H = \frac{(1+\mathrm{sgn}(\bar{K}^{\mathrm{m}}_{\mathrm{HII}}(\mathrm{t})))}{2}\ (G^{\mathrm{max}}_H - G^{\mathrm{nom}}_H) + \frac{(1-\mathrm{sgn}(\bar{K}^{\mathrm{m}}_{\mathrm{HII}}(\mathrm{t})))}{2}\ (G^{\mathrm{nom}}_H - G^{\mathrm{min}}_H)$ is the weighting factor to bound the scaling gain within the allowable limits (i.e. between G^{min}_H and G^{max}_H), where $\mathrm{sgn}(x)$ is the sign function of x.

Once the scaling gain for human force is estimated, (3) can be rewritten as follows:

$$Y(s) =\ \frac{G_E}{\tau_a s+1} \tag{8}$$

where $G_E =\ G_H\, K_a$ is the effective admittance gain of the controller.

We can deduce that altering the force scaling gain G_H affects both admittance damping and inertia at the same rate, resulting no change in the admittance time constant.

IV. Stability Limits

A. Stability

Stable interaction is mandatory for any pHRI system, but the trade-off between stability and transparency has to be balanced well for optimal task performance [35]. To ensure stability, we inspect the pole locations of the closed-loop transfer function, T(s), given in (1) for a range of gain (K_a) and time constant (τ_a) values of the admittance controller while keeping $G_{\mathrm{H}} =\ 1$. For this purpose, we need the transfer function models of robot and human arm impedance. We utilize UR5 (Universal Robots Inc.) as the collaborative robot in our study. Since the manufacturer does not supply the dynamical model of the robot, we rely on the transfer function model, $G(s)$, estimated by Aydin *et al.* [34]. The dynamical behavior of human arm is nonlinear, time and configuration dependent. However, it is a commonly used simplifying assumption that the impedance of human arm, $Z_H(s)$, can be described by a linearized mass-spring-damper model (see [12], [33], [34]) as $Z_H\ (s) =\ m_H s + b_H + k_H/s$, where m_H, b_H, and k_H are the human arm endpoint mass, damping and stiffness, respectively. Although exact dynamics of human arm is unknown, the parameters of human arm impedance typically reside within specific limits. In light of the literature [36], [37], [38], the upper bound for human arm stiffness k_H is taken as 600 N/m, and the lower and upper bounds for the mass parameter m_H are taken as 0.1 and 5 kg, respectively, while the limits for the damping b_H are set to 0.1 and 41 Ns/m. For each extreme combination of parameters of human arm impedance (m_H, b_H, k_H), stable sets of controller parameters (K_a, τ_a) are computed and stability boundaries are determined. Then, as suggested in [39], [40], the parameters (K_a, τ_a) corresponding to the conservative regions, where the stability is ensured under each extreme combination of human arm impedance parameters (m_H , b_H, k_H), are considered as the stable controller parameters (see Fig. 5). Note that these parameters are valid for the case in which the robot motion is not significantly affected by the environment (see Section II).

B. Maximum Amplification

In the above analysis, the stable region of controller parameters are determined while keeping $G_H =\ 1$. To determine the upper bound of G_H that can be used for maximum force amplification, we investigate the gain margin of the system under each set of (K_a, τ_a) in the stable region of Fig. 5. The contour plot of G_{H} values in this region is depicted in Fig. 6. From Fig. 6, we can observe that, for each time constant τ_a, amount of allowable change in amplification depends on the value of admittance gain K_a. Moreover, for a given K_a, there is an optimal admittance time constant, where the force amplification is maximum. In Fig. 6, this value is $\tau^{\mathrm{opt}}_a =\ 0.054$, which can be used to determine the maximum allowable

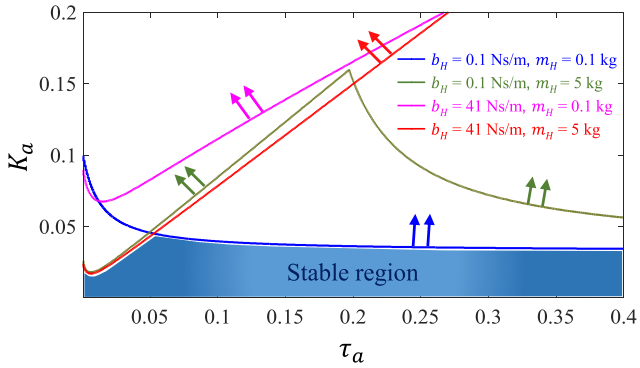

Fig. 5. Stability maps of the pHRI system for $k_H = 600$ N/m. The curves represent the stability boundaries for different combinations of human arm impedance parameters m_H and b_H. The shaded area represents the sets of effective gain and time constant values that ensure stability for all bounds of m_H and b_H. Directions of the arrows refer to unstable regions for each set of m_H and b_H.

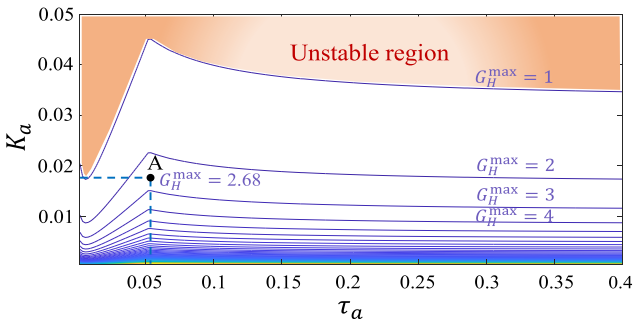

Fig. 6. Gain margin for the sets of controller parameters (K_a, τ_a) in the stable region.

amplification gain, $G_H^{\max}$, and hence the maximum effective controller gain, $G_E^{\max}$. For example, let's assume that the parameters of an admittance controller are $(K_a, \tau_a^{\text{opt}}) = (0.0167,\ 0.054)$ and the gain margin of the corresponding closed loop system is 2.68 (see point A in Fig. 6). Hence, the maximum allowable amplification gain is $G_H^{\max} = 2.68$. Accordingly, the maximum effective controller gain is $G_E^{\max} = G_H^{\max}\ K_a = 0.0448$.

V. Experiment

We designed and conducted a pHRI experiment to investigate the following research questions:

Q1: Is there an optimum admittance time constant that maximizes human force amplification in pHRI for the proposed gain profile (Fig. 3b)?

Q2: Does the proposed admittance gain profile leads to a more effective co-manipulation in terms of task performance than the ones suggested in the literature?

A. Experimental Set-up

The main components of the set-up used for our pHRI experiment (see Fig. 7) consists of a collaborative robot (UR5, Universal Robot Inc.), a mobile cart that is rigidly connected to the robot and moving on a rail and carrying a mass of 26 kg

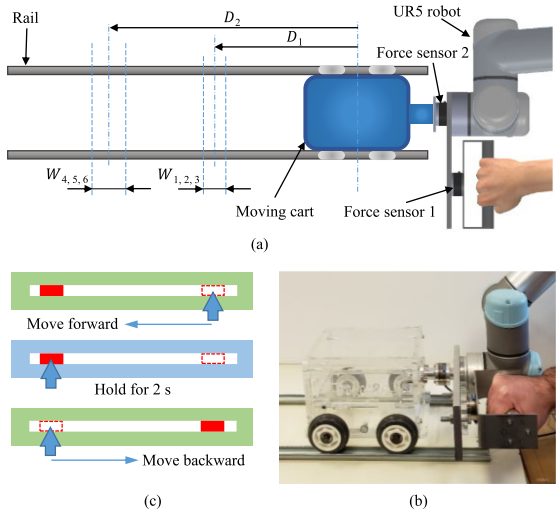

Fig. 7. The experimental setup [(a), (b)] and visual feedback provided to subjects during the experiment (c).

(note that the mass is not shown in Fig. 7b), and two force sensors (Mini40, ATI Inc.), each measuring the force applied by subject and robot to the cart separately (see Fig. 7a, 7b). All experimental data was acquired at 125 Hz (the update rate of the closed-loop control system shown in Fig. 2) by a DAQ card (USB-6343, National Instruments Inc.). During the experiments, the instantaneous force applied to the cart by a subject is scaled up/down according her/his movement intention and then fed to the admittance controller, which outputs a desired velocity for the cart. The robot aims to push the cart with this desired velocity until a new force input comes from the subject (see the control architecture in Fig. 2).

B. Experimental Procedure

Subjects were asked to grasp the handle shown in Fig. 7a and move the cart from a starting point to a parking zone as fast and accurate as possible. Subjects were asked to perform the task in both directions; in one trial, they pushed the cart forward, and in the successive trial, they pulled it backward. A visual feedback was provided to subjects during the experiment by displaying a moving cursor on a computer screen, emulating the movements of cart (see Fig. 7c). Subjects were asked to hold the cart stable in the parking zone for 2 seconds. A time counter was displayed through the computer screen and triggered when they entered the parking zone for the first time. During this dwell time, if subject maintained the cart position successfully without overshooting outside the parking zone, a prompt "start to the next trial" appeared on the computer screen, and the next trial began. Otherwise, the time counter restarted at every overshoot, and the additional overshooting time was added to the movement time as a penalty.

C. Participants

Nine subjects (3 females and 6 males whose age vary between 20 and 40 with an average of 26) participated in the experiment. Subjects gave informed consent about their

TABLE I
FITTS' TASK DESIGN PARAMETERS

Parking width W (cm) = D / (2^{ID} - 1) Shanoon formula		Index of dificulty ID (bits)		
		4	5	6
Distance D (cm)	$D_1 = 25$	$W_1 = 1.667$	$W_2 = 0.81$	$W_3 = 0.4$
	$D_2 = 40$	$W_4 = 2.667$	$W_5 = 1.29$	$W_6 = 0.635$

participation in the experiment. The experimental study was approved by the Ethical Committee for Human Participants of Koc University.

D. Experimental Design

The experiment was designed to imitate Fitts's reaching movement task [41]. Fitts's reaching task requires a rapid movement from a starting point to a target area. This task is designed specifically to investigate speed-accuracy trade-off characteristics of human muscle movement with some analogy to Shannon's channel capacity theorem. As the aim in most co-manipulation tasks such as ours is to reduce human effort while maximizing manipulation accuracy, Fitts's reaching task offers utilization of well-established measures to characterize task performance. In particular, a linear relationship between movement time MT and index of task difficulty ID has been suggested by Fitts [41], $\mathrm{MT} = a + b\,\mathrm{ID}$. The empirical coefficients a and b depend on environment and controller. The index of difficulty (in bits) is a function of reaching distance D and parking width W through Shannon formula [42], $\mathrm{ID} = \log_2(D/W + 1)$. Following these relations, we designed the experiment by considering three indices of difficulties ($\mathrm{ID} = 4$, 5, and 6 bits) and two reaching distances ($D = 25$, and 40 cm). This design results in six different parking widths as listed in Table I.

E. Performance Measures

We used the average power consumed by subject ($P^{\mathrm{ave}} = 1/(t_f - t_i)\int_{t_i}^{t_f} |f_H(t).v(t)|dt$), average force applied by subject ($F_H^{\mathrm{ave}} = 1/(t_f - t_i)\int_{t_i}^{t_f} |f_H(t)|dt$) [33], average force applied by robot to move the cart ($F_R^{\mathrm{ave}} = 1/(t_f - t_i)\int_{t_i}^{t_f} |f_R(t)|dt$), average velocity of the cart ($\{V^{\mathrm{ave}} = 1/(t_f - t_i)\int_{t_i}^{t_f} |v(t)|dt$), and the movement time MT as measures to evaluate the task performance. In the expressions above, t_i and t_f were the time when the cart velocity just exceeded 2% of the maximal velocity of the trial and the time when the cart entered the parking zone, respectively [19]. The movement time MT was quantified by measuring the time starting from t_i till finishing the trial after removing the dwell time [19].

We calculated the ratio, $\eta = F_R^{\mathrm{ave}}/F_H^{\mathrm{ave}}$, to evaluate the relative force contribution of the robot to the task. Moreover, to evaluate the parking accuracy, we calculated the parking overshoot, which was, for a single trial, the number of times the manipulated object left and reentered the target zone during parking before the trial was finished successfully [19]. Then, parking overshoot was computed for each subject by summing up the number of reentries for all trials of that subject for each ID divided by the total number of trials of that ID.

F. Regarding Q1: Verification of the optimum time constant

As the theoretical analysis in the previous section has shown, there is an optimal time constant, τ_a^{opt}, that maximizes the amplification capacity of human force. In this section, we report the empirical evidence to support this finding. We designed an experimental study to investigate the effect of time constant on the performance of our pHRI system. In our experiment, we used an admittance controller utilizing the proposed adaptive force amplification gain profile with six different time constants, including values below and above τ_a^{opt}. These conditions are labeled as τ_1, τ_2, $\tau_3 (= \tau_a^{\mathrm{opt}})$, τ_4, τ_5, and τ_6, corresponding to the time constant values of 0.03, 0.04, 0.054, 0.08, 0.1, and 0.2, respectively. For a given nominal admittance gain $K_a = 0.0167$, the permissible maximum amplification gain $G_H^{\max}$ for each admittance time constant was obtained from the gain margin plot (Fig. 6) as 1.78, 2.18, 2.68, 2.46, 2.37, and 2.17 for τ_1, τ_2, τ_3, τ_4, τ_5, and τ_6, respectively. For all conditions, the desired profile of the adaptive controller starts from the same nominal amplification gain $G_H^{\mathrm{nom}} = 1$ and ends at the same minimum amplification (i.e., maximum attenuation) gain $G_H^{\min} = 0.33$. Other parameters are taken as $\alpha = 20$, $\Delta t = 0.008\,\mathrm{s}$.

In this experiment, each experimental condition was repeated 8 times for each parking width W given in Table I. Thus, there were a total of 288 (6 conditions x 6 parking widths x 8 repetitions) trials in the experiment. Each subject conducted the experiment in four sessions; 72 (6 conditions x 6 parking widths x 2 repetitions) trials per session. The trials of each session were randomized while the same order was displayed to each subject. In addition, subjects were given a training set of 12 (6 conditions x 2 parking widths x 1 repetition) trials prior to each session.

G. Regarding Q2: Comparing the proposed adaptive gain profile with the other profiles suggested in the literature

To investigate the potential benefits of proposed admittance controller with adaptive force scaling utilizing the proposed gain profile (labelled as C1), we compared it with two different admittance controllers; C2 and C3 (see Fig. 8). Note that $K_a = 0.0167$ and $\tau_a^{opt} = 0.054$ were used as the nominal admittance parameters in all controllers. As shown in Fig. 4d, the desired gain profile for C1 relies on three critical values; first, the nominal force scaling gain G_H^{nom}, which is the value at the start of motion. Second is the maximum force scaling gain $G_H^{\max}$, which is obtained from the gain margin plots in Fig. 6. The last is the minimum force scaling gain (i.e., maximum attenuation) $G_H^{\min}$, which is used during the parking phase. In our implementation of the gain profile for C1, the values given in Table II were utilized.

In addition to the controller given above, we explored the effect of different gain profiles suggested in the literature on the task performance. These alternative profiles, C2 and C3,

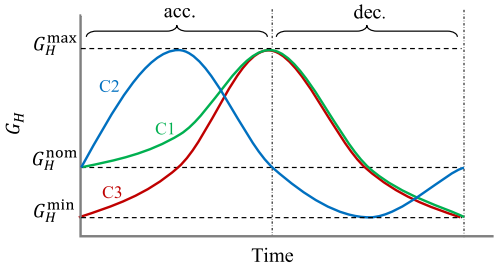

Fig. 8. Representative gain profiles for the controllers tested in our study. C1 is the proposed adaptation gain profile, while C2 and C3 are similar to the profiles resulted from the adaptive approaches introduced in [22]–[25], and [13, 26], respectively. Please note that the gain profiles C2 and C3 for force scaling are mirror images of the damping profiles suggested in the related references.

TABLE II
PARAMETER VALUES FOR THE CONTROLLER C1

(K_a, τ_a^{opt})	G_H^{nom}	$G_H^{\max}$	$G_H^{\min}$	α	Δt
(0.0167, 0.054)	1	2.68	0.33	20	0.008

have been suggested in the literature to adjust the dissipation capacity of an admittance controller by varying the admittance damping. In C2, which was adopted from the earlier studies in [22]–[25], the amplification (attenuation) occurrs only during the acceleration (deceleration) (see Fig. 8). Although the force scaling gain varied between the maximum $G_H^{\max}$ and minimum $G_H^{\min}$ values in C2, the nominal value (i.e., G_H^{nom}) was used during both the starting and parking phases. On the other hand, C3, which was adopted from the studies in [13] and [26], represents a gain profile where high amplification was provided to the operator during the driving phase (see Fig. 8) though $G_H^{\min}$ was used during both the starting and parking phases.

In summary, three controllers were tested in this experiment utilizing different adaptive gain profiles (C1, C2, and C3). Each controller case was repeated 8 times for each parking width W given in Table I. Thus, there were a total of 144 (3 controllers x 6 parking widths x 8 repetitions) trials in the experiment. Each subject conducted the experiment in four sessions; 36 (3 controllers x 6 parking widths x 2 repetitions) trials per session. The trials of each session were randomized while the same order was displayed to each subject. In addition, subjects were given a training set of 6 (3 controllers x 2 parking widths x 1 repetition) trials prior to each session.

H. Data Analysis:

The performance measures defined in Sect. V-E were computed and the means and standard errors of the means were evaluated. All dependent variables (i.e., measures) were tested for normality using the Shapiro–Wilk test. We found that the distribution was non-normal for some of the measures. Normalizing transformations were applied to the measures as suggested in [43]. A two-way ANOVA was conducted to examine the effects of index of difficulty (ID) and admittance time constant (τ) regarding Q1, and controller type regarding Q2, on each performance measure. A significance level of p = 0.05 was used to test the null hypothesis in the statistical analysis.

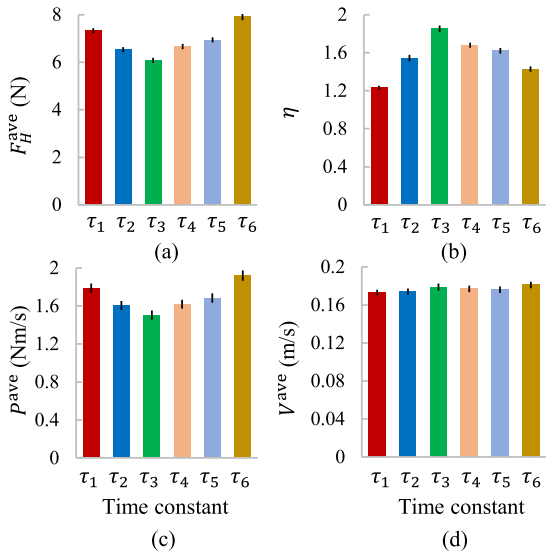

Fig. 9. The means and standard errors of the means of the performance measures; (a) average force applied by subjects F_H^{ave}, (b) relative force contribution of the robot η, (c) average power consumed by subjects P^{ave}, and (d) average velocity of the cart V^{ave} for six admittance time constants τ_1, τ_2, τ_3, τ_4, τ_5, and τ_6.

Regarding Q1: There was a statistically significant interaction between ID and τ on parking overshoot and movement time (MT). Therefore, we examined the simple main effects of ID and τ on both parking overshoot and MT. On the other hand, no significant interaction was observed between the effects of ID and τ on F_H^{ave}, η, P^{ave}, and V^{ave}. So, we selected the Tukey post-hoc test to investigate the effect of admittance time constant τ on these measures. The mean values of subjects for all measures are reported in Figs. 9 and 10.

Regarding Q2: In the analyses, we found a significant interaction between the experimental factors (ID and controller type) for all measures. Therefore, further analysis was performed to evaluate the individual simple main effects of ID and controller type. Fig. 11 illustrates the results of our second experiment which was designed to compare the proposed gain profile (C1) with the ones proposed in the literature (C2 and C3).

I. Results and Discussion:

Regarding Q1: Figs. 9a, 9b, 9c, and 9d report the average force applied by subjects F_H^{ave}, the relative contribution of the robot in task execution η, the average power consumed by subjects P^{ave}, and the average velocity V^{ave}, respectively. These plots were obtained for each performance measure under each admittance time constant τ by averaging the results of all ID levels. Post-hoc comparisons using the Tukey test indicated that F_H^{ave} (η) under $\tau_3 (= \tau_a^{\text{opt}})$ was significantly lower (higher) than those of all other admittance time constants. Furthermore, P^{ave} under τ_3 was significantly lower than those of τ_1, τ_5, and τ_6. Although P^{ave} under τ_3 was lower than those of τ_2 and τ_4 as well, the difference was not statistically significant. The effect of admittance time constant on V^{ave} was not statistically significant.

As depicted in Fig. 10a, parking overshoot under τ_3 was not significantly different than those of the others for ID = 4.

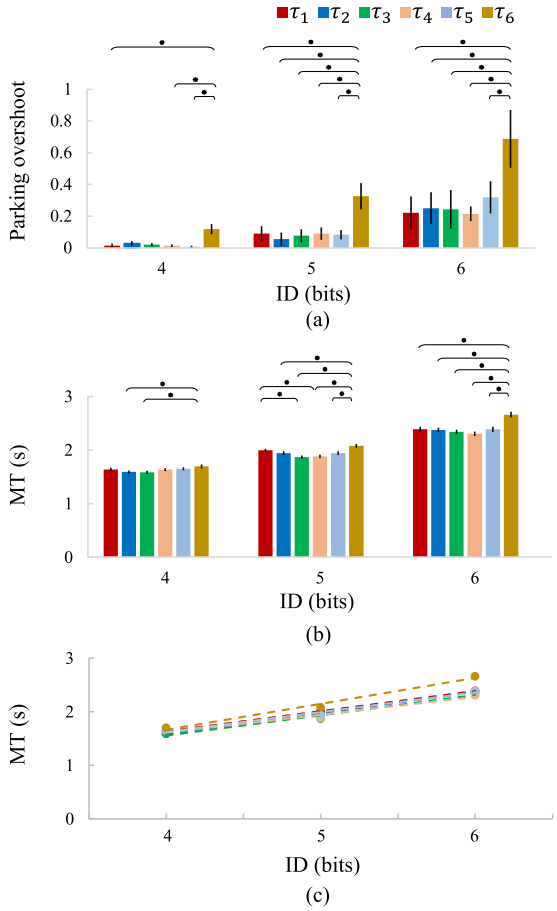

Fig. 10. The means and standard errors of means of the performance measures; (a) parking overshoot, (b) MT, and (c) linear regression between ID and MT for six admittance time constants τ_1, τ_2, τ_3, τ_4, τ_5, and τ_6. Horizontal bracket with * on top indicates statistical significance between the results of the two corresponding conditions.

Furthermore, the differences between the parking overshoots under τ_1, τ_2, τ_3, τ_4, and τ_5 were not significant for ID $= 5$ and ID $= 6$, while parking overshoot under τ_6 was significantly higher than those of the others.

Fig. 10b illustrates the movement time MT for different IDs. MT under τ_3 was significantly lower than that of τ_6 (those of τ_1 and τ_6) for ID $= 4$ (for ID $= 5$). For ID $= 6$, MT under τ_6 was significantly higher than those of the others.

For each time constant, the relation between MT and ID was linear ($\mathrm{MT} = a + b\,\mathrm{ID}$) with a high R-squared value (see Table III), which indicates that Fitts's law is also valid for a dissipative environment as suggested in [19]. The linear relationship between MT and ID shows that the slopes b under τ_1-τ_5 were similar (see Fig. 10c), as listed in Table III. On the other hand, the slope of τ_6 was higher since the controller under τ_6 utilizes a higher admittance time constant. Furthermore, the slope, b, is reciprocally related to the information transmission rate (i.e., index of performance). Specifically, the index of performance (i.e., IP $= 1/b$) describes the information transmitted to subjects per unit time to successfully perform the task [19], [44]. As expected, IP was lower under τ_6 than those of the others since a high time constant causes sluggish response. This increases the possibility of overshooting at higher ID (see Fig. 10a), which in turn increases task duration, and the slope. As expected, movement time MT depicted in Fig. 10b showed that subjects completed the task significantly slower under τ_6 than those of τ_1-τ_5, especially at higher ID. Although subjects were moving in a relatively similar speed under all time constants considered in this experiment (see Fig. 9d), they completed the task with more overshoots under τ_6 compared to those of the others, which led to longer MT.

As shown in Figs. 9a-9c, τ_3 transcended τ_1, τ_2, τ_4, τ_5, and τ_6 in terms of F_H^{ave}, η, and P^{ave}. These experimental results support our theoretical analysis in Section IV and our claim that there is an optimal time constant ($\tau_3 = \tau_a^{\mathrm{opt}}$) maximizing the human force amplification.

This experiment also highlighted the difference in the performance between the conditions of low and high time constant. For instance, $\tau_2 = 0.04$ and $\tau_6 = 0.2$ have almost the same allowable force amplification of 2.18 and 2.17, respectively. However, the results depicted in Figs. 9 and 10 showed that τ_2 significantly outperformed τ_6 in all performance measures since increasing the time constant reduces the response speed of an admittance controller. As a result, an object having a high inertia cannot be accelerated easily [25], requiring more effort from human operator. Furthermore, once the object is accelerated, it is difficult to decelerate it as well. Hence, overshoot during parking is unavoidable.

Regarding Q2: Figs. 11a and 11c depict the average force applied by subjects, F_H^{ave}, and the relative force contribution of the robot to task, η, respectively. F_H^{ave} (η) under C1 was significantly lower (higher) than those of C2 and C3 for each ID. The average force applied by robot, F_R^{ave}, is plotted in Fig. 11b. F_R^{ave} under C2 was significantly lower than those of C1 and C3 for each ID. However, F_R^{ave} under C3 was significantly higher than that of C1 for ID $= 4$. The average velocity of the cart, V^{ave}, is plotted in Fig. 11d. V^{ave} under C2 was significantly lower than those of C1 and C3. Fig. 11e illustrates the average power consumed by subjects, P^{ave}, which was significantly lower under C1 than those of C2 and C3 for ID $= 4$. Fig. 11f reports the results for parking overshoot. Parking overshoot under C2 was significantly higher than those of C1 and C3 for ID $= 6$. As shown in Fig. 11g, the movement time MT under C2 was significantly higher than those of C1 and C3 for each ID.

We observed that subjects completed the task with higher MT under C2 than those of C1 and C3 for all IDs (see Fig. 11h). This is because C2 resulted in higher dissipation than C1 and C3 (see Fig. 8), which caused the robot to resist the movements of subjects, and hence an increase in task duration. Moreover, the index of performance IP under C2 was lower than those of C1 and C3 (see Table IV), which showed that less information per unit time was transmitted to subjects to perform the task successfully under C2 than those of C1 and C3.

Fig. 11c shows that the relative force contribution of robot to task, η, was significantly higher under C1 than those of C2 and C3 for each ID, which indicates that subjects applied less force to move the cart under C1. Fig. 11d shows that subjects moved the cart with higher velocity under C1 and C3 than that of C2 for each ID. Since the effort made by subjects is quantified as force times velocity,

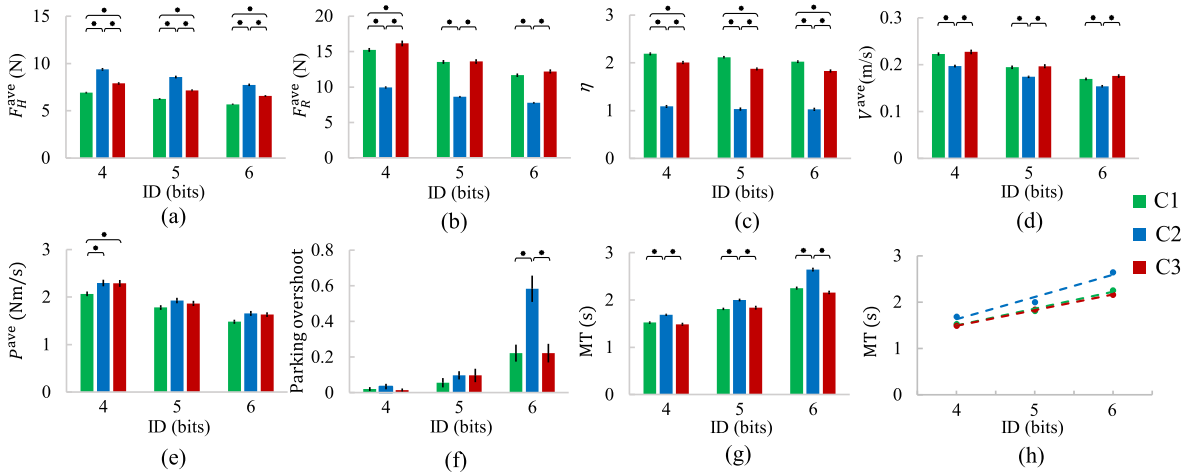

Fig. 11. Mean values of the performance measures for three different IDs under three different controllers C1 (our proposed controller), C2, and C3. Error bars are the standard errors of means and horizontal bracket with * on top indicates statistical significance between the results of the two corresponding controllers.

TABLE III
PARAMETERS OF THE LINEAR REGRESSION BETWEEN MT AND ID FOR THE ADMITTANCE TIME CONSTANTS τ_1, τ_2, τ_3, τ_4, τ_5, AND τ_6

Conditions	a	b	IP (1/b)	R^2
τ_1	0.133	0.375	2.67	0.99
τ_2	0.014	0.392	2.55	0.99
τ_3	0.041	0.378	2.64	0.98
τ_4	0.273	0.334	2.99	0.97
τ_5	0.151	0.369	2.71	0.98
τ_6	- 0.266	0.483	2.07	0.98

TABLE IV
PARAMETERS OF THE LINEAR REGRESSION BETWEEN MT AND ID FOR THE CONTROLLERS C1, C2, AND C3

Controller	a	b	IP (1/b)	R^2
C1	0.045	0.363	2.75	0.98
C2	- 0.28	0.478	2.09	0.96
C3	0.15	0.335	2.98	0.99

subjects put significantly less effort under C1 than those of C2 and C3. Moreover, parking accuracy under C2 was lower than those of C1 and C3 when index of difficulty was high since the gain profile of C2 ends with a non-conservative gain value (i.e., G_H^{nom}), causing a lower dissipation than those of C1 and C3. C1 and C3 allowed subjects to end the task with the maximum attenuation gain $G_H^{\min}$, which provided more dissipation at the parking phase to position the cart accurately (see Fig. 8).

VI. DISCUSSION

To summarize above, the results of the experiments provide us with satisfactory answers to the research questions (Q1 and Q2) posed at the beginning of Section V.

Specifically, adaptive force scaling controller utilizing $\tau_3 = \tau_a^{\text{opt}}$ significantly outperformed those under τ_1, τ_2, τ_4, τ_5, and τ_6 in terms of F_H^{ave}, η, and P^{ave}. Hence, empirical evidence for an optimum admittance time constant was provided, which reinforce our theoretical analysis in Section IV.

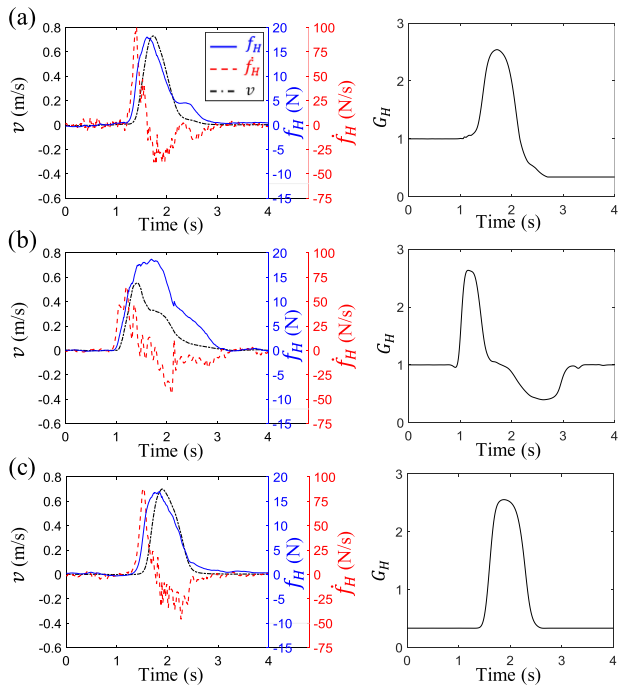

Fig. 12. Cart velocity v, force applied by human f_H, its derivative $\dot{f}_H$, and adaptive gain G_H, as functions of time for exemplary trials of one subject under the controllers of (a) C1 (our proposed controller), (b) C2, and (c) C3.

Moreover, in terms of the gain profile, adaptive admittance gain used in C1 is more desirable than those suggested in the literature (C2 and C3). In particular, the proposed profile results in lower F_H^{ave} and P^{ave} and higher η than those calculated for C2 and C3. In addition, parking accuracy under C1 was better than that of C2, whereas C1 and C3 performed similarly, as anticipated. When the effort made by subjects to move the cart and parking accuracy are considered together, C1 outperformed C2 and C3.

Fig. 12a shows the actual gain profile recorded for one subject under C1 during one of the experimental trials. It indeed follows a trend similar to the desired gain profile suggested in Sect. III (see Fig. 3b). This shows that our approach successfully

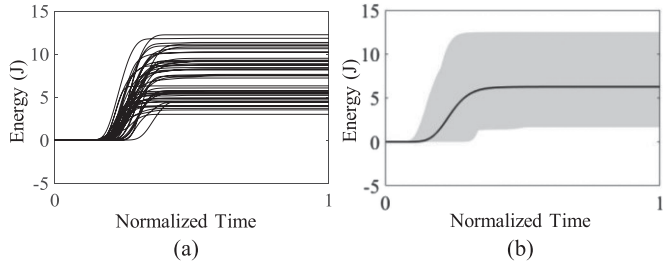

Fig. 13. (a) Energy exchange for one subject as a function of normalized time (solid curves represent the individual trials), (b) Average energy exchange of all subjects (solid curve) under the proposed controller C1. The minimum and maximum energies of all trials for all subjects at each time step were utilized to construct the boundaries of the shaded region.

combines human intention and the different requirements of task phases as proposed in this study.

As shown in Fig 12a, the scaling gain increased from its nominal value till it reached its permissible upper limit during the driving phase, allowing maximum assistance to the subject for acceleration. Once a deceleration intention of the subject was detected, the gain gradually decreased to a minimum value (i.e., maximum attenuation), allowing the subject to decelerate the cart. As soon as the parking started, a high level of attenuation for the force was already reached, allowing the subject to park the cart more accurately.

Altering the gain in real-time can pose a threat in terms of stability if the instantaneous change in gain is too abrupt. There is a passivity approach suggested in the literature [45] to monitor the energy exchange during real-time pHRI. In Fig. 13, we present the estimated energy exchange for all trials of one subject and also the average of all subjects under the proposed controller C1. This figure illustrates that the monitored energy never goes below zero in any of the trials, and hence the passivity is maintained.

Finally, although there are no particular restrictions in applying the proposed approach to more realistic pHRI scenarios involving point-to-point manipulation of objects in 3D space, tuning in some parameters may be required depending on the task. In the future, we plan to work on a 3D co-manipulation task in which a user and robot lift a heavy object together and put it on a shelf. Our aim is to reduce the effort made by the user during the lifting by adjusting the force scaling gain on the fly using the proposed approach.

VII. Conclusion

In this study, we proposed an approach for adaptive scaling of human force based on predicted human intention to achieve more effective co-manipulation in terms of task performance during pHRI. The proposed approach interprets human intention as to accelerate and decelerate the manipulated object while paying attention to the different phases of pHRI task. Human intention was quantified by a numerical value, which was then used to adapt the gain of an admittance controller without affecting its time-constant. The results of the first set of experiments provided evidence to the existence of an optimum admittance time constant for a given co-transportation task. Moreover, the results of the second set of experiments suggested that the proposed profile for gain adaptation is superior to the ones proposed in the literature for the same purpose. In addition, the linear relation obtained between the movement time MT and the index of difficulty ID in both experiments suggested that Fitts's law is also valid for a pHRI task involving co-transportation of an object. In the future, we aim to test our approach in more realistic pHRI scenarios involving contact interactions with an environment to further demonstrate its potential in industrial applications [35][46]. Instead of using a rail system, virtual fixtures can be utilized to constrain the movements of manipulated object in those scenarios.

Acknowledgment

Yahya M. Hamad acknowledges University of Baghdad for financially supporting him during his PhD studies. The Scientific and Technological Research Council of Turkey (TUBITAK) supported this work under contract EEEAG-117E645.

References

[1] J. Kruger, T. K. Lien, and A. Verl, "Cooperation of human and machines in assembly lines," *CIRP Ann. Manuf. Technol.*, vol. 58, no. 2, pp. 628–646, 2009.
[2] S. Y. Lee, K. Y. Lee, S. H. Lee, J. W. Kim, and C. S. Han, "Human–robot cooperation control for installing heavy construction materials," *Auton. Robots*, vol. 22, pp. 305–319, 2007.
[3] S. Lee and J. Il Moon, "Introduction of human-robot cooperation technology at construction sites," in *Proc. Int. Symp. Automat. Robot. Construction Mining (ISAR)*, vol. 31, 2014, pp. 1–6.
[4] T. Wojtara *et al.*, "Human-robot collaboration in precise positioning of a three-dimensional object," *Automatica*, vol. 45, no. 2, pp. 333–342, 2009.
[5] A. Mortl *et al.*, "The role of roles: physical cooperation between humans and robots," *Int. J. Robot. Res.*, vol. 31, no. 13, pp. 1656–1674, 2012.
[6] J. Ernesto Solanes *et al.*, "Human–robot collaboration for safe object transportation using force feedback," *Robot. Auton. Syst.*, 107, pp. 196–208, 2018.
[7] J. Han, S. Lee, and J. Kim, "Behavior hierarchy-based affordance map for recognition of human intention and its application to human–robot interaction," *IEEE Trans. Hum.–Mach. Syst.*, vol. 46, no. 5, pp. 708–722, Oct., 2016.
[8] A. Kucukyilmaz, T. Sezgin, and C. Basdogan, "Intention recognition for dynamic role exchange in haptic collaboration," *IEEE Trans. Haptics*, vol. 6, no. 1, pp. 58–68, First Quarter, 2013.
[9] H. Kazerooni and S. Mahoney, "Force augmentation in human-robot interaction," in *Proc. Amer. Control Conf.*, 1990, , pp. 2821–2826.
[10] N. Abroug, X. Lamy, and E. Laroche, "Human force augmentation: optimal control parameters tuning using structured H∞ synthesis," in *Proc. IEEE Int. Conf. Intell. Robots Syst.*, 2016, pp. 702–709.
[11] B. Cagneau, G. Morel, D. Bellot, N. Zemiti, and G. d'Agostino, "A passive force amplifier," in *Proc. IEEE Int. Conf. Robot. Automat.*, 2008, pp. 2079–2084.
[12] R. Ikeura, T. Moriguchi, and K. Mizutani, "Optimal variable impedance control for a robot and its application to lifting an object with a human," in *Proc. IEEE Int. Workshop Robot Hum. Interactive Commun.*, 2002, pp. 500–505.
[13] G. Kang, H. S. Oh, J. K. Seo, U. Kim, and H. R. Choi, "Variable admittance control of robot manipulators based on human intention," in *IEEE/ASME Trans. Mechatronics*, vol. 24, no. 3, pp. 1023–1032, Jun. 2019.
[14] T. Tsumugiwa, R. Yokogawa, K. Hara, "Variable impedance control based on estimation of human arm stiffness for human-robot cooperative calligraphic task," in *Proc. IEEE Int. Conf. Robot. Autom.*, 2002, pp. 644–650.
[15] M. Rahman, R. Ikeura and K. Mizutani, "Investigating the impedance characteristics of human arm for development of robots to cooperate with human operators," in *Proc. IEEE Int. Conf. Syst., Man, Cybern.*, 1999, pp. 676–681.

[16] L. Peternel, N. Tsagarakis, and A. Ajoudani, "A human-robot co-manipulation approach based on human sensorimotor information," *IEEE Trans. Neural Syst. Rehabil. Eng.*, vol. 25, no. 7, pp. 811–822, Jul. 2017.
[17] S. Grafakos, F. Dimeas, and N. Aspragathos, "Variable admittance control in pHRI using EMG-based arm muscles co-activation," *in Proc. IEEE Int. Conf. Syst., Man, Cybern.*, 2016, pp. 1900–1905.
[18] D. Sirintuna, I. Ozdamar, Y. Aydin, and C. Basdogan, "Detecting human motion intention during pHRI using artificial neural networks trained by EMG signals," in *Proc. IEEE Int. Conf. Robot Hum. Interactive Commun. (Ro-Man)*, 2020, pp. 1280–1287.
[19] A. Keemink *et al.*, "Using position dependent damping forces around reaching targets for transporting heavy objects: A Fitts' law approach," in *Proc. 6th IEEE Int. Conf. Biomed. Robot. Biomechatronics (BioRob)*, 2016, pp. 1323–1329.
[20] H.-Y. Li *et al.*, "Stable and compliant motion of physical human robot interaction coupled with a moving environment using variable admittance and adaptive control," *IEEE Robot. Automat. Lett.*, vol. 3, no. 3, pp. 2493–2500, Jul. 2018.
[21] H.-Y. Li., T. Nuradha, S. A. Xavier, U-X. Tan, "Towards a compliant and accurate cooperative micromanipulator using variable admittance control," in *Proc. IEEE 3rd Int. Conf. Adv. Robot. Mechatronics*, 2018, pp. 230–235, 2018.
[22] V. Duchaine and C. M. Gosselin, "General model of human-robot cooperation using a novel velocity based variable impedance control," in *Proc. Joint EuroHaptics Conf. Symp.*, 2007, pp. 446–451.
[23] V. Duchaine, B. Mayer-St-Onge, D. Gao, and C. Gosselin, "Stable and intuitive control of an intelligent assist device," *IEEE Trans. Haptics*, vol. 5, no. 2, pp. 1939–1412, Apr.–Jun., 2012.
[24] Y. Aydin, N. Arghavani, and C. Basdogan, "A new control architecture for physical human-robot interaction based on haptic communication," in *Proc. ACM/IEEE Int. Conf. Hum.- Robot Interaction*, 2014, pp. 122–123.
[25] A. Lecours, B. Mayer-St-Onge, and C. Gosselin, "Variable admittance control of a four-degree-of-freedom intelligent assist device," in *Proc. IEEE Int. Conf. Robot. Automat.*, 2012, pp. 3903–3908.
[26] F. Dimeas and N. Aspragathos, "Fuzzy learning variable admittance control for human-robot cooperation," in *Proc. IEEE Int. Conf. Intell. Robots Syst.*, 2014, pp. 4770–4775.
[27] P.D. Labrecque, C. Gosselin, "Variable admittance for pHRI: from intuitive unilateral interaction to optimal bilateral force amplification," *Robot. Comput. Integr. Manuf.*, vol. 52, 2018, pp. 1–8.
[28] X. Lamy, F. Colledani, F. Geffard, Y. Measson, and G. Morel, "Human force amplification with industrial robot: study of dynamic limitations," in *Proc. IEEE/RSJ Int. Conf. Intell. Robots Syst.*, 2010, pp. 2487–2494.
[29] K. Kosuge, Y. Fujisawa, and T. Fukuda, "Control of robot directly maneuvered by operator," in *Proc. IEEE/RSJ Int. Conf. Intell. Robots Syst.*, 1993, pp. 49–54.
[30] C. Luna, M. Rahman, M. Saad, P. Archambault, and S. Ferrer, "Admittance-based upper limb robotic active and active-assistive movements," *Int. J. Adv. Robot. Syst.*, vol. 12, no. 9, pp. 117–130, 2015.
[31] L.M. Miller and J. Rosen, "Comparison of multi-sensor admittance control in joint space and task space for a seven degree of freedom upper limb exoskeleton," in *Proc. IEEE/RAS-EMBS Int. Conf. Biomed. Robot. Biomechatronics*, 2010, pp. 70–75.
[32] R. Goljat, J. Babic, T. Petric, L. Peternel, and J. Morimoto, "Power-augmentation control approach for arm exoskeleton based on human muscular manipulability," *in Proc. IEEE Int. Conf. Robot. Automat.)*, 2017, pp. 5929–5934.
[33] Y. Aydin, O. Tokatli, V. Patoglu, and C. Basdogan, "Fractional order admittance control for physical human-robot interaction," in *Proc. IEEE World Haptics Conf.*, 2017, pp. 257–262.
[34] Y. Aydin, O. Tokatli, V. Patoglu, and C. Basdogan., "Stable physical human-robot interaction using fractional order admittance control," *IEEE Trans. Haptics*, vol. 11, no. 3, pp. 464–475, Jul.–Sep. 2018.
[35] Y. Aydin, O. Tokatli, V. Patoglu, and C. Basdogan, "A computational multi-criteria optimization approach to controller design for physical human-robot interaction," *IEEE Trans. Robot.*, vol. 6, no. 6, pp. 1791–1804, Dec. 2020.
[36] S. P. Buerger and N. Hogan, "Complementary stability and loop shaping for improved human–robot interaction," *IEEE Trans. Robot.*, vol. 23, no. 2, pp. 232–244, Apr. 2007.
[37] J. M. Dolan, M. B. Friedman, and M. L. Nagurka, "Dynamic and loaded impedance components in the maintenance of human arm posture," *IEEE Trans. Syst., Man, Cybern.*, vol. 23, no. 3, pp. 698–709, May/Jun., 1993.
[38] T. Tsuji, P. Morasso, K. Goto, and K. Ito, "Human hand impedance characteristics during maintained posture in multi-joint arm movements," *Biol. Cybern.*, vol. 72, pp. 476–485, 1995.
[39] B. Willaert, M. Franken, H. V. Brussel, and E. B. V. Poorten, "On the use of shunt impedances versus bounded environment passivity for teleoperation systems," in *Proc. IEEE Int. Conf. Robot. Automat.*, 2011, pp. 2111–2117.
[40] Y. Aydin, D. Sirintuna, and C. Basdogan, "Towards collaborative drilling with a cobot using admittance controller," *Trans. Inst. Meas. Control*, vol. 43, no. 8, pp. 1760–1773, Jul. 2020.
[41] P. M. Fitts, "The information capacity of the human motor system in controlling the amplitude of movement," *J. Exp. Psychol.*, vol. 47, no. 6, pp. 381–391, 1954.
[42] R. W. Soukoreff and I. S. MacKenzie, "Towards a standard for pointing device evaluation, perspectives on 27 years of Fitts' law research in HCI," *Int. J. Hum.-Comput. Stud.*, vol. 61, no. 6, pp. 751–789, 2004.
[43] G. F. Templeton, "A two-step approach for transforming continuous variables to normal: Implications and recommendations for IS research," *Commun. Assoc. for Inf. Syst.*, vol. 28, pp. 41–58, 2011.
[44] I. S. MacKenzie, "Fitts' law as a research and design tool in human-computer interaction," *Hum. Comput. Interaction*, vol. 7, pp. 91–139, 1992.
[45] J. Ryu, D. Kwon, and B. Hannaford, "Stability guaranteed control: time domain passivity approach," *IEEE Trans. Control Syst. Technol.*, vol. 12, no. 6, pp. 860–868, Nov. 2004.
[46] D. Sirintuna, Y. Aydin, O. Caldiran, O. Tokatli, V. Patoglu, and C. Basdogan, "A variable-fractional order admittance controller for pHRI," *Proc. IEEE Int. Conf. Robot. Automat.*, 2020, pp. 10162–10168.

Yahya M. Hamad received the B.Sc. and M.Sc. degrees from the University of Baghdad, Baghdad, Iraq, in 1997 and 2000, respectively, both in mechanical engineering. He is currently working toward the Ph.D. degree with the Mechanical Engineering Department, Koc University, Istanbul, Turkey. His research interests include robotics, physical human-robot interaction, and applied mechanics.

Yusuf Aydin (Member, IEEE) received the B.Sc. dual degrees in mechanical engineering and electrical and electronics engineering, the M.Sc. degree in mechanical engineering, and the Ph.D. degree in mechanical engineering from Koc University, Istanbul, Turkey, in 2011, 2013, and 2019, respectively. He is currently a Faculty Member with the Electrical and Electronics Engineering Program, MEF University, Istanbul, Turkey. Before joining MEF University, he was a Postdoctoral Research Fellow with Robotics and Mechatronics Laboratory, Koc University. His research interests include physical human-robot interaction, haptics, robotics, control, optimization, and mechatronics. He was the recipient of the prestigious TUBITAK BIDEB Fellowship for his graduate studies.

Cagatay Basdogan (Member, IEEE) received the Ph.D. degree in mechanical engineering from Southern Methodist University, Dallas, TX, USA, in 1994. He is currently a Faculty Member with the Mechanical Engineering and Computational Sciences and Engineering Programs, Koc University, Istanbul, Turkey. He is also the Director of Robotics and Mechatronics Laboratory, Koc University. Before joining Koc University, he was with NASAJPL/Caltech, MIT, and Northwestern University Research Park. His research interests include haptic interfaces, robotics, mechatronics, biomechanics, medical simulation, computer graphics, and multimodal virtual environments. He was an Associate Editor in Chief of the IEEE TRANSACTIONS ON HAPTICS and is currently on the Editorial Boards of the IEEE TRANSACTIONS ON MECHATRONICS, PRESENCE*: Teleoperators and Virtual Environments, and Computer Animation and Virtual Worlds* Journals. In addition to serving in programme and organizational committees of several conferences, he chaired the IEEE World Haptics Conference in 2011.